www.springer.com/41230
https://doi.org/10.1007/s41230-025-4117-5
Research & Development
Vol. 23 No. 4 July 2026
CHINA FOUNDRY

# Grain refinement and dendrite morphology of superalloy K4169 during equiaxed growth under pulsed magnetic field

**Ce Zheng[1], Yue-fei Teng[1,2], Fu-qiang Wang[3], *Ying-ju Li[1], Tian-jiao Luo[1], Xiao-hui Feng[1], Cheng Zhu[1], and **Yuan-sheng Yang[1]**

*1. Institute of Metal Research, Chinese Academy of Sciences, Shenyang 110016, China*

*2. AECC Commercial Aircraft Engine Co., Ltd., Shanghai 201306, China*

*3. Shenyang Aircraft Industry (Group) Co., Ltd., Shenyang 110850, China*



**Abstract:** The grain refinement effect of superalloy K4169 under a low-voltage pulsed magnetic field (PMF) with different pulse frequencies and pulse voltages, at a superheat of 191 °C, was investigated. The grains of the ingots are refined, decreasing from 3.9 mm without the application of PMF to 1.7 mm with PMF. Furthermore, the dendrite morphology undergoes a transformation, changing from well-developed branches to a global rosette pattern with rounded dendrite tips. However, it is worth noting that the secondary dendrite arm spacing increases under the influence of PMF. The refinement mechanism was investigated by quenching experiments and theoretical analysis under PMF. The high superheat of 191 °C results in a low cooling rate and a small thermal gradient during solidification, which promotes the survival of heterogeneous nuclei, leading to grain refinement. Additionally, evolutions in dendrite morphology are attributed to increased heterogeneous nucleation. When PMF is applied, the solidification structure is refined even under high superheat conditions. This leads to simultaneous improvements in filling ability and grain size refinement, offering promising applications for the practical manufacturing of thin-walled complex parts.

**Keywords:** Ni-based superalloy; pulsed magnetic field; grain refinement; dendrite morphology; solidification

**CLC numbers:** TG146.1⁺5 **Document code:** A **Article ID:** 1672-6421(2026)04-523-12

## 1 Introduction

K4169 is one of the most widely used nickel-based superalloys in gas turbines, rocket motors, spacecraft, nuclear reactors, pumps, and toolings due to its good mechanical properties and high corrosion resistance at elevated temperatures[1]. Fine, isotropic equiaxed grains are the most promising solidification structures for K4169 castings. Thus, the grain refinement of K4169 by adding grain refiners such as Co-Fe-Nb and Cr-Mo-Nb[2] or using special fine-grain casting methods[3] is one of the most interesting topics for manufacturers and researchers. As an alternative method for grain refinement, the application of electromagnetic fields during the solidification of metallic alloys has been widely investigated in the past few decades[4]. Plenty of research works have been carried out on the grain refinement of various alloys under various types of electromagnetic fields[5-9].

Recently, a low-voltage pulsed magnetic field (PMF) has been developed to refine the solidification structure of various metals and alloys, with minimal modifications required to existing manufacturing equipment and processes. This innovative approach has been investigated in magnesium alloys[10], aluminum alloys[11], silicon steels[12], and superalloys[13-14]. For superalloy IN718, Ma et al.[15] found, under a low-voltage PMF, the best refinement effect could be obtained under the pulse frequency of 5 Hz and the pulse voltage of 200 V. Li et al.[16] further investigated the effect of mold temperature and superheating on the grain refinement

***Ying-ju Li**

Male, Ph. D., Professor. His research interests primarily focus on the mechanism of microstructure refinement of superalloys under pulsed magnetic field conditions.

E-mail: yjli@imr.ac.cn

****Yuan-sheng Yang**

E-mail: ysyang@imr.ac.cn

Received: 2024-05-31; Revised: 2024-07-31; Accepted: 2025-01-02

under a PMF, which indicated that the refinement effect was improved with the decrease of the cooling rate and the melt superheating. Mold nucleation experiments[13] and sieve experiments[15] were carried out to investigate the refinement mechanism under a PMF, which showed that grain refinement was caused by the multiplication of heterogeneous nuclei from the chilling mold wall. Numerical simulation was also employed to clarify the physical mechanisms under a PMF. Interestingly, a periodic electromagnetic force was generated by PMF, causing vibration and forced fluid flow in the melt[16]. By synchrotron X-ray radiography investigation, Liotti et al.[17] observed the fragmentations of dendrite tips and secondary dendrite arms under a PMF. All the above works focused on the effects of the magnetic field while neglecting the influence of thermal effects.

Previous works also inferred that a low-voltage PMF could not promise a grain refinement in K4169 when the pouring temperature exceeds 1,430 °C and the mold temperature below 800 °C[16, 18]. Ma et al.[18] explained that if the pouring temperature was too high, for example 1,430 °C, the heterogeneous nuclei detached from the mold wall would be remelted, so that the grain refinement effect was not apparent under those thermal conditions. Therefore, it is necessary to investigate the grain refinement behavior and mechanism under a PMF at high temperatures, which is favorable for the production of castings with thin walls.

In this work, the grain refinement of the as-cast superalloy K4169 was achieved under a low-voltage PMF with a high pouring temperature of 1,550 °C, which corresponded to a superheat of 191 °C. Theoretical calculations were conducted to investigate the grain refinement mechanisms, encompassing nucleation-free energy, nucleus proliferation, and the survival of free crystal nuclei. Additionally, the study explored suitable thermal conditions conducive to grain refinement. In addition, the evolution of dendrite morphology under a PMF was discussed in detail.

# 2 Experimental procedure

The nickel-based casting alloy K4169 was used in the experiments. Its chemical compositions (wt.%) are 0.05 C, 0.01 Co, 52 Ni, 3.05 Mo, 5.3 Nb, 8.4 Cr, 0.55 Al, 1.05 Ti, and balanced Fe. K4169 master alloy was remelted using an induction furnace (VMI-25F) and then poured, at 1,550 °C, into an investment mold preheated to 950 °C to cast a cylinder ingot with a diameter of *Φ*50 mm and a length of 70 mm. The superheating was 191 °C, which can generally satisfy the filling conditions of superalloy casting products[19].

After pouring, the melt was solidified under a low voltage PMF with four different pulse frequencies (0 Hz, 2.5 Hz, 5 Hz, 10 Hz) and three pulse voltages (70 V, 140 V, 200 V). The specimens were transversely sectioned near the bottom of the ingot, and then were ground, polished, and etched. For grain observation, the samples were etched in a solution consisting of 30 g $CuSO_4$, 100 mL HCl, and 7 mL $H_2SO_4$. For dendrite morphology analysis, electrolytic etching was carried out using a solution containing 10 mL $HNO_3$, 30 mL HCl, and 50 mL $C_3H_8O_3$. The microstructures were observed by optical microscopy (Lecai-MEF4A).

# 3 Results

## 3.1 Effect of pulse frequency on macrostructure of K4169 superalloy

The horizontal macrostructure of solidified K4169 superalloy under the PMF at pulse frequencies of 0 Hz, 2.5 Hz, 5 Hz, and 10 Hz, with a fixed pulse voltage of 200 V, is shown in Fig. 1. It can be seen that the solidified structure of K4169 without PMF exhibits a coarse equiaxed-grain structure, with similar grain sizes at both the edges and centers, as shown in Fig. 1(a). When a PMF with a frequency of 2.5 Hz is applied, the solidified structure is refined to a certain degree, especially for the grains in the center, as shown in Fig. 1(b). When the pulse frequency increases to 5 Hz, the grain refinement effect is more obviously than that of 2.5 Hz, as shown in Fig. 1(c). However, the larger equiaxed grains appear in the edge of solidification structure as the pulse frequency further increases to 10 Hz, indicating that the refinement effect weakens, as shown in Fig. 1(d). The average grain size on the cross-section of the ingot as a function of pulse frequency is shown in Fig. 2, which shows the similar trend with macrostructures in Fig. 1. The average grain size decrease from 3.9 mm without the PMF to 1.7 mm with PMF under frequency of 5 Hz.

Figure 3 shows the dendritic morphology of solidification structure in the ingot's central region under the PMFs with different pulse frequencies and a fixed pulse voltage of 200 V. When the pulse frequencies increase from 2.5 Hz to 10 Hz, the morphologies of the dendrites undergo significant degradation:

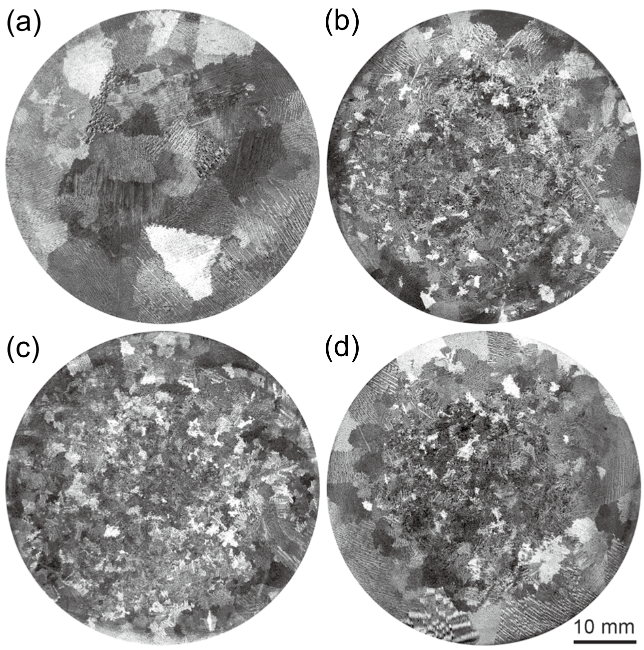


**Fig. 1: As-cast macrostructure of K4169 superalloy under different pulse frequencies: (a) 0 Hz; (b) 2.5 Hz; (c) 5 Hz; (d) 10 Hz**

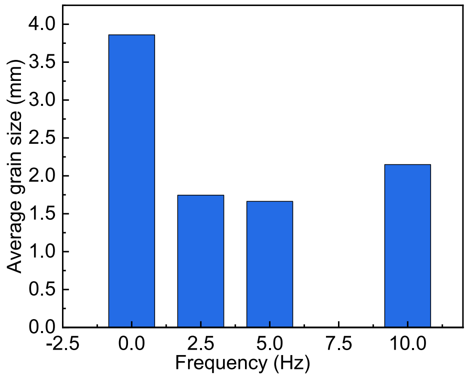


**Fig. 2: Average grain size of K4169 superalloy with different pulse frequencies**

the dendrite tips become blunt, the dendritic morphology becomes incomplete, and the secondary arm spacing increases [Figs. 3(b, d)]. Specially, the degradation of dendritic morphology is most pronounced at a PMF frequency of 5 Hz [Fig. 3(c)].

## 3.2 Effect of pulse voltage on microstructure of K4169 superalloy

Figure 4 shows the solidification structure of K4169 with different pulse voltages at a pulse frequency of 5 Hz. The solidification structure under PMF with a pulse voltage of 70 V is not well refined compared with 0 V maybe due to the intensity of pulse field is too low. Compared with the solidification

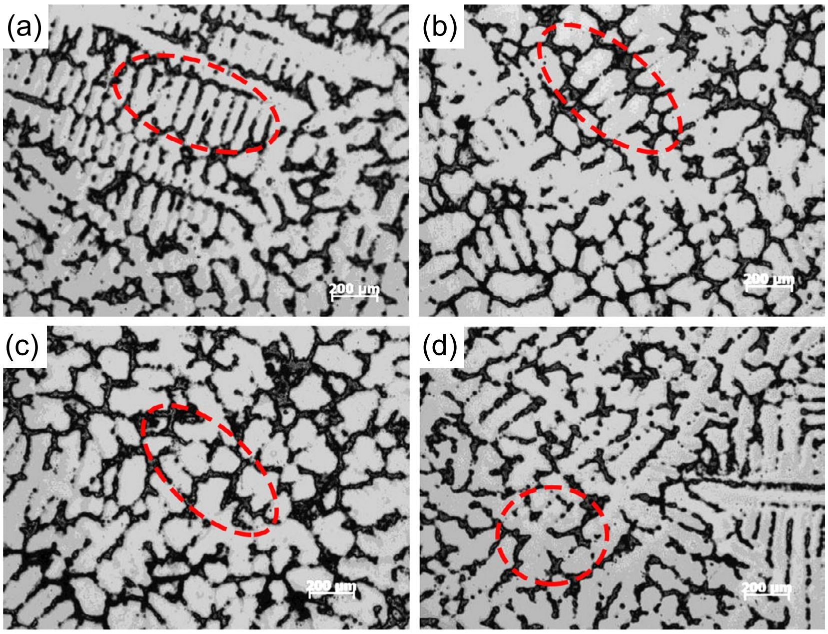


**Fig. 3: Dendrite structures under PMFs with different pulse frequencies under a pulse voltage of 200 V: (a) 0 Hz; (b) 2.5 Hz; (c) 5 Hz; (d) 10 Hz**

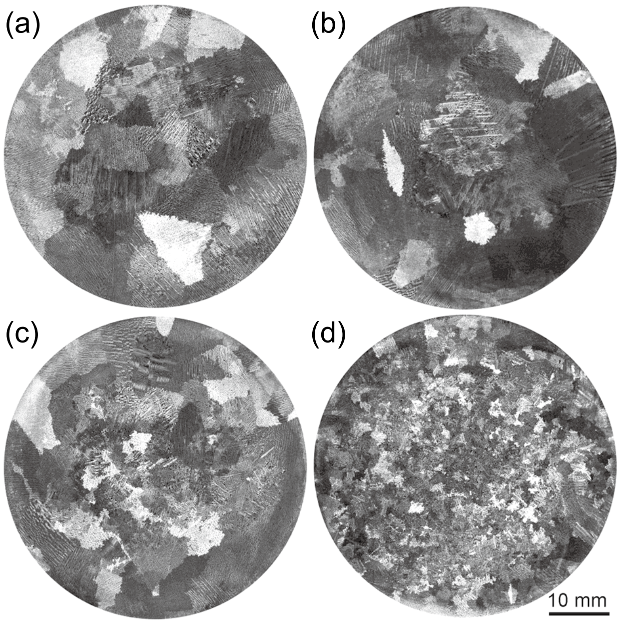


**Fig. 4: As-cast macrostructures of K4169 superalloy under different pulse voltages at a pulse frequency of 5 Hz: (a) 0 V; (b) 70 V; (c) 140 V; (d) 200 V**

structure under PMF with a pulse voltage of 70 V [Fig. 4(b)], the grains in the central region of ingot, under a pulse voltage of 140 V [Fig. 4(c)], are effectively refined. When the pulse voltage further increases to 200 V, the grains of the entire ingot are refined, resulting in fine equiaxed crystals [Fig. 4(d)]. As shown in Fig. 5, the grain size is decreased from 4.0 mm to 1.7 mm as the pulse voltage increases from 70 V to 200 V.

Figure 6 shows the dendritic morphology of the solidification structure in the central region of the ingot under the PMFs with different pulse voltages at a pulse frequency of 5 Hz. From Fig. 6, it is noted that without PMF, the solidification structure is consisted of well-developed dendrites [Fig. 6(a)]. When the pulse voltage is 70 V, there is no significant change in the dendritic morphology [Fig. 6(b)]. However, when the pulse voltage increases to 140 V, the dendritic morphology gradually degrades, accompanied by an increase in the secondary dendrite arm spacing [Fig. 6(c)]. When the pulse voltage further increases to 200 V, the morphology of the dendrites severely degrades. The dendrite tips undergo passivation, causing the dendrites to become fragmented [Fig. 6(d)].

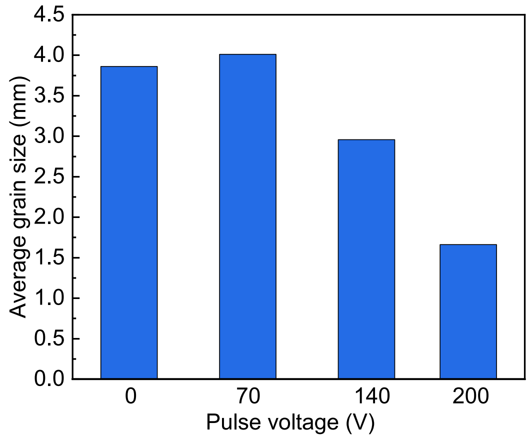


Fig. 5: Average grain sizes of K4169 superalloy with different pulse voltages

# 4 Discussion

## 4.1 Refinement mechanism under PMF

### 4.1.1 Grain refinement in different stages of solidification under PMF

The cooling curve of the K4169 superalloy melt was measured using a tungsten-rhenium thermocouple positioned 15 mm from the bottom along the central axis of the ingot. Based on the recorded cooling curve, the solidificastion process of the alloy was invided into three stages, as shown in Fig. 7(a). Subsequently, a PMF with a frequency of 5 Hz and a pulse voltage of 200 V was applied in four different modes: (1) throughout the entire solidification process; (2) during the pure liquid phase stage; (3) during the solidification platform stage; and (4) during the later stage of solidification.

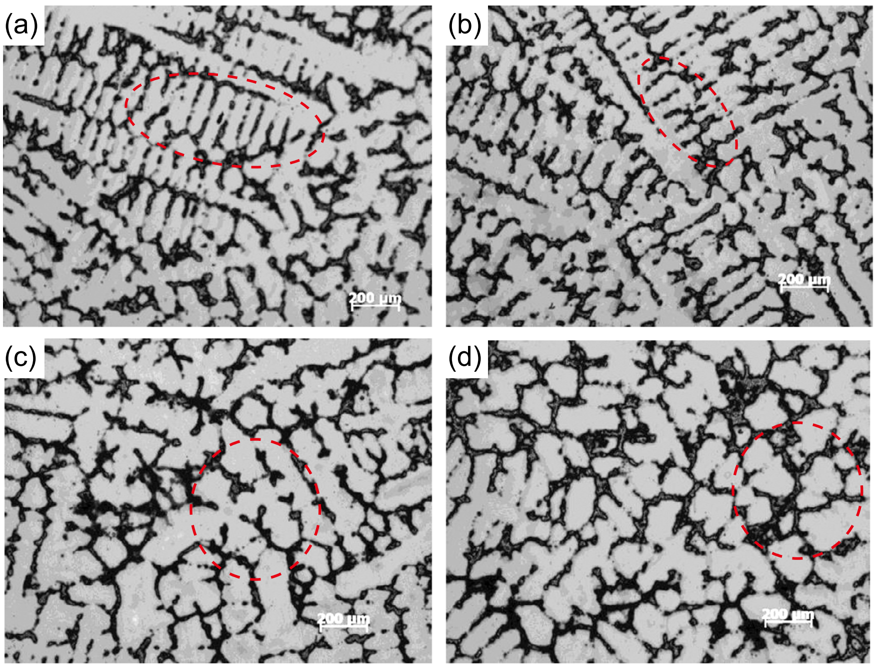


Fig. 6: Dendrite structures under PMFs with different pulse voltages and a pulse frequency of 5 Hz: (a) 0 V; (b) 70 V; (c) 140 V; (d) 200 V

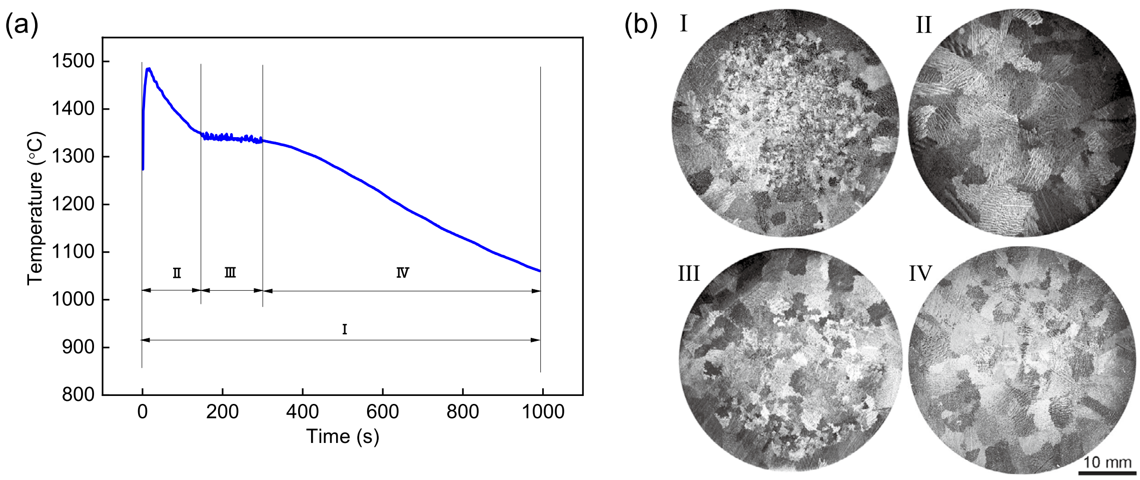


Fig. 7: Cooling curve at the center of the transversal section 15 mm from the bottom (a) and as-cast macrostructures with PMF applied at different solidification stages (b)

From Fig. 7(b), it can be seen that refined equiaxed grains are obtained by applying PMF throughout the entire solidification process (Stage I). The equiaxed grains are still relatively coarse when the PMF is only applied in the pure liquid phase (Stage II). When the PMF is applied only during the solidification platform stage (Stage III), there is a noticeable grain refinement effect. However, this refinement effect is not as significant as when the PMF is applied throughout the entire solidification process (Stage I). When PMF is only applied during the later stage of solidification (Stage IV), the grain refinement effect is not apparent.

The above results show that the PMF has a grain refinement effect on the K4169 superalloy mainly during the liquid-solid transition stage (nucleation stage), consistent with the previous experimental results of other alloys[11, 12]. It can be concluded that the application of PMF during the solidification should be on the nucleation process of crystals, rather than on the growth process of dendrites.

### 4.1.2 Effect of PMF on nucleation-free energy

According to the results in Fig. 7, the main reason for the grain refinement effect of PMF is its influence on the nucleation process. Thus, the impact of PMF on the free energy of the liquid-solid phase transition was analyzed. According to the classical nucleation theory, when a crystal nucleus appears in the liquid phase under the action of PMF, the change in Gibbs free energy of the system consists of three parts: the difference in Gibbs free energy between the volume of the liquid phase and the solid phase $\Delta G_V$, free energy provided by PMF $\Delta G_{PMF}$, and solid-liquid interface $\Delta G_i$. The total Gibbs free energy change of the system is represented by Eq. (1):

$$\Delta G = \Delta G_V + \Delta G_{PMF} + \Delta G_i = \left(\Delta G_V + \Delta G_{pmf}\right)V + \sigma_{LS}A \quad (1)$$

where $\Delta G_V$ represents the Gibbs free energy difference and $\Delta G_{pmf}$ denotes the free energy provided by PMF, as shown in Eqs. (2) and (3)[20]. $V$ and $A$ represent the volume and surface area of the crystal nucleus, respectively. $\sigma_{LS}$ represents the solid-liquid interfacial tension.

$$\Delta G_V = \frac{\Delta H_V \Delta T}{T_m} \quad (2)$$

$$\Delta G_{pmf} = \frac{1}{2}\vec{H}\cdot\vec{B} = \frac{1}{2\mu_m}\left|\vec{B}\right|^2 \quad (3)$$

where $\Delta H_V$ is the latent heat of solidification, $\Delta T$ is the degree of undercooling, $T_m$ is the melting point, $\vec{H}$ is the magnetic field intensity vector, $\vec{B}$ is the magnetic flux density vector, $\mu_m$ is the changes in magnetic permeability during liquid-solid transition of materials.

When the crystal nucleus is a spherical shape with a radius of $r$:

$$\Delta G = \left|\frac{\Delta H_V \Delta T}{T_m} + \frac{1}{2\mu_m}\left|\vec{B}\right|^2\right|\frac{4}{3}\pi r^3 + \sigma_{LS}4\pi r^2 \quad (4)$$

According to Eq. (4), the Gibbs free energy of the system shows a trend of first increasing and then decreasing with the increase of the nucleus radius $r$. When the nucleus radius is greater than the critical nucleus radius $r^*$, the Gibbs free energy decreases with the increase of the nucleus radius, indicating that the nucleus can continue to grow. Take the derivative of Eq. (4) over $r$, so that $d\Delta G/dr=0$, the critical nucleus radius under the action of a PMF is represented by Eq. (5):

$$r^* = -2\sigma_{LS} / \left(\frac{\Delta H_V \Delta T}{T_m} + \frac{1}{2\mu_m}\left|\vec{B}\right|^2\right) \quad (5)$$

The percentage decrease in critical nucleus radius, $P_r$, after applying a PMF is represented by Eq. (6):

$$P_r = \frac{r^*_{ori} - r^*}{r^*_{ori}} = 1 - \frac{1}{1 + \frac{T_m\left|\vec{B}\right|^2}{\Delta H_V \Delta T 2\mu_m}} \quad (6)$$

where $r^*_{ori}$ represents the critical nucleus radius when no PMF is applied.

Nucleation work $\Delta G^*$ is shown in Eq. (7):

$$\Delta G^* = \frac{16}{3}\pi\sigma_{LS}^3 / \left(\frac{\Delta H_V \Delta T}{T_m} + \frac{1}{2\mu_m}\left|\vec{B}\right|^2\right)^2 \quad (7)$$

The percentage decrease in nucleation work $P_G$ caused by a PMF is represented by Eq. (8):

$$P_G = \frac{\Delta G^*_{ori} - \Delta G^*}{\Delta G^*_{ori}} = 1 - \left(\frac{1}{1 + \frac{T_m\left|\vec{B}\right|^2}{\Delta H_V \Delta T 2\mu_m}}\right)^2 \quad (8)$$

where $\Delta G^*_{ori}$ represents the nucleation work without PMF.

Based on the various parameters of physical properties of K4169, $\Delta H_V$=2.6×10$^9$, $T_m$=1,632 °C, $\mu_m$=4π×10$^{-7}$[21]. The variation curves of $P_r$ and $P_G$ with magnetic induction intensity under different degrees of undercooling are shown in Fig. 8.

As shown in Fig. 8, the influence of PMF on critical nucleation radius and nucleation work increases with an increase in magnetic induction intensity. When the undercooling is small, it significantly impacts the critical nucleation radius and nucleation work, even if the magnetic induction intensity is low. However, the influence of PMF on the critical nucleation radius and nucleation work becomes weaker as the undercooling increases. Therefore, the critical nucleation radius decreases under the action of PMF, as well as the required nucleation work with an increase in undercooling. Considering the existence of crystal nuclei with different sizes in liquid-phase metals, assuming that the number and size distribution of these nuclei do not change after applying PMF, the decrease in critical nucleus radius and nucleation work means that smaller nuclei can continue to grow and eventually form grains, increasing the number of nuclei. This leads to an increase in the number of nuclei and the refinement of grains under the action of PMF.

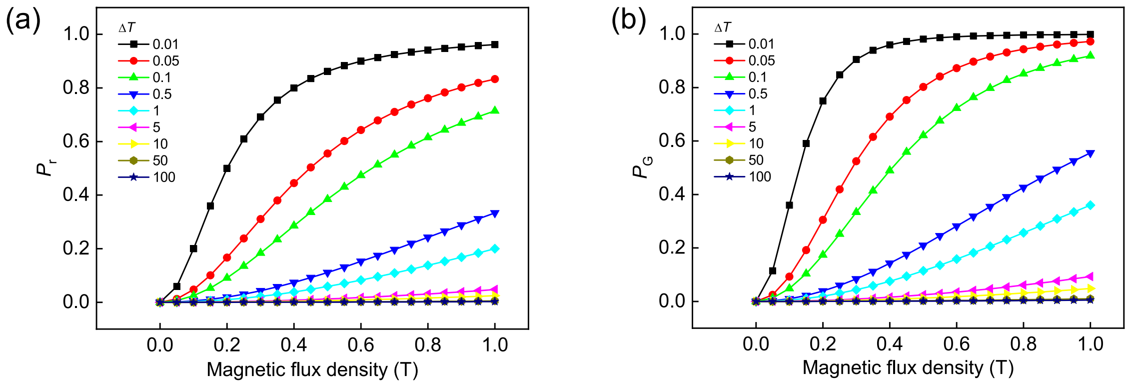


**Fig. 8: Effect of magnetic flux density on nucleation under different supercooling: (a) percentage decrease in critical nucleation radius ($P_r$); (b) percentage decrease in nucleation energy ($P_G$)**

### 4.1.3 Nucleus proliferation under the action of PMF

The experimental results of applying a PMF at different stages of solidification indicate that the PMF mainly plays a refining role in the liquid-solid transition stage, which is primarily focused on crystal nucleation. The energy fluctuations provided by the PMF give a driving force for the liquid-solid transition process, which may be one of the reasons for the refinement of grains under the PMF. In addition, the proliferation of crystal nuclei caused by PMF may also be one of the reasons for the refinement of grains. The grain structure between the screen mesh and the mold wall is significantly refined, while the grain structure inside the screen mesh is poorly refined under the action of PMF. In addition, Ma et al.[18] found that the grain refinement effect of the PMF was more pronounced when a rough-surface corundum mold was used, compared to a smooth-surface quartz mold. Based on the observed results, it is believed that the primary refining mechanism involves the movement of crystal nuclei from the mold surface into the melt. This movement is facilitated by the forced convection and oscillation generated by the application of PMF. Consequently, this process leads to an increase in heterogeneous nucleation at the center of the samples.

Further analysis was conducted on the process of dendrite fragmentation and survival under the action of PMF. Firstly, considering the fragmentation and dissociation of dendrites during the solidification process, it is necessary to describe the morphological characteristics of the solidification structure. According to the correspondence between cooling conditions and microstructure in solidification theory[20], the morphology characteristics of solidified microstructure are determined by cooling conditions, without considering the influence of solute elements. The cooling conditions of the melt include cooling rate $R$, temperature gradient $G$, and dendritic growth rate $V$. The relationship among the three conditions should satisfy Eq. (9):

$$R = G \times V \tag{9}$$

According to solidification theory, when a crystal grows in a dendritic morphology, the growth rate and temperature gradient have an impact on the spacing between primary dendrites $\lambda_1$, and secondary dendrite arm spacing $\lambda_2$, as follows[22]:

$$\begin{cases} \lambda_1 \propto G^{-1/2} V^{-1/4} \\ \lambda_2 \propto (G \times V)^{-1/3} \end{cases} \tag{10}$$

Under the action of PMF, the flow velocity of the melt perpendicular to the growth direction of the dendrite arm is $u$, and when the melt comes into contact with the dendrite arm, all the momentum perpendicular to the direction of the dendrite arm is transferred to the arm. Within a very short time interval $\Delta t$, it is assumed that the velocity direction changes once the molten metal flow at a certain rate contacts the dendritic arm. This assumption does not account for the forces generated by the molten metal flow that oppose the direction of the flow on the dendritic arm. When the dendritic arm simplified as a cylinder, the impulse received by the entire dendritic arm is equal to the decrease in the momentum of the fluid in this direction according to the law of conservation of momentum. As shown in Fig. 9, the force acting on the segment of the dendritic arm with a length of $L$ and a diameter of $\lambda$ is expressed by Eq. (11):

$$F \cdot \Delta t = \int_0^{\pi} (u - u\cos\theta) \cdot (\rho L (u\Delta t) \frac{\lambda}{2} \mathrm{d}\theta \sin\theta) \tag{11}$$

where $\rho$ is the density of K4169 alloy, $\mathrm{d}\theta\sin\theta$ represents the mass of the molten dendrite arm comes into contact within an range $\mathrm{d}\theta$ at angle $\theta$ during the time interval $\Delta t$.

$$F = \rho L \lambda u^2 \tag{12}$$

The shear strength of the dendritic arm is expressed as $\sigma_{crit}$. When the stress ($\sigma$) at the root of the dendritic arm is greater than its shear strength of $\sigma_{crit}$, the dendritic arm can be broken.

$$\sigma = \frac{F}{\frac{1}{4}\pi\lambda^2} = \frac{4\rho L u^2}{\pi\lambda} > \sigma_{crit} \tag{13}$$

According to Flemings' discussion on the properties of metals in the semi-solid state[23], the strength of metals is low near the liquidus. For example, Dahle et al.[24] found that the strength of aluminum alloys in a semi-solid state is $10^3$–$10^4$ Pa. According to the dendritic morphology shown in Figs. 3 and 6, the length $L$ and space $\lambda$ of the dendritic arm are approximately 300 μm and 20 μm, respectively. When the melt flow velocity $u$ is 0.1 m·s$^{-1}$, the stress at the root of the dendritic arm is about $10^4$ Pa based on Eq. (13). In addition, due to the presence of solid-liquid phases in the mushy zone, the resistivity of the solid phase is about half of that of the liquid phase. Under the action of PMF, the amplitude of oscillation between the solid and liquid phases is different, which may cause turbulence in the mushy

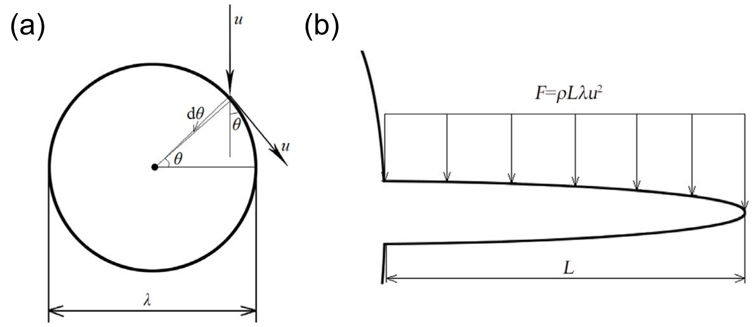


**Fig. 9: Mechanism analysis of dendrite arms based on the conservation of momentum: (a) transverse section of dendrite arm; (b) entire dendrite arm**

zone. Meanwhile, the enrichment of solutes in the melt near the root of the dendrite arm and the lower solidification point may lead to a necking phenomenon occurring at the root of the dendrite arm, resulting in a decrease in the cross-sectional area of the dendrite arm during the growth process of dendrites. According to Eq. (13), shear strength of the dendritic arm $\sigma_{crit}$ is half due to the reduced diameter of dendritic arm caused by necking. Considering the above factors, the fracture of dendritic arms caused by melt flow is possible. From the above analysis, it can also be seen that the chilled dendrites on the surface of the mold may also detach under the action of PMF. Moreover, due to the absence of metal bonds between the dendrites and the surface of the mold, the bonding force is weaker than that between the dendrite arms and the dendrite roots. Therefore, the detachment of quenched dendrites on the surface of the mold is easier under the PMF.

Meanwhile, the cooling conditions greatly influence the critical melt flow velocity, causing dendrite fracture. According to Eq. (10), the length of dendritic arms strongly correlates with the spacing between primary dendrites. In contrast, the diameter of dendritic arms strongly correlates with the spacing between secondary dendrites. Using growth rate and temperature gradient to approximate the length and diameter of dendrite arms, Eqs. (14) and (15) are obtained:

$$L = k_2 G^{n_1} V^{n_2} \tag{14}$$

$$\lambda = k_3 G^{n_3} V^{n_4} \tag{15}$$

where $k_2$, $k_3$, $n_1$, $n_2$, $n_3$, and $n_4$ are all undetermined coefficients, with $n_1$ is approximately −1/2, $n_2$ is approximately −1/4, $n_3$ is approximately −1/3, and $n_4$ is approximately −1/3.

The relationship between the flow velocity of the melt ($u$), growth rate ($V$), and temperature gradient ($G$) needs to satisfy Eq. (16):

$$u > \sqrt{\frac{1}{4}\pi\frac{\lambda\sigma_{crit}}{\rho L}} = k_{fracture} G^{n_5} V^{n_6} \tag{16}$$

where $k_{fracture}$, $n_5$, and $n_6$ are all undetermined coefficients, and $n_5$ is approximately 1/12 and $n_6$ is approximately −1/24.

The flow pattern of the mushy zone is very complex, which is difficult to accurately describe the flow situation of the melt at different positions. When no PMF is applied, natural convection exists in the melt. In situ observation also found that broken dendritic arms appeared in some positions without PMF[17]. Under the action of PMF, the melt flow becomes more intense, and the number of broken dendritic arms increases[17], indicating that the flow velocity at more positions satisfies Eq. (16). It can be inferred that the forced convection becomes more intense under a stronger PMF, resulting in more dendritic arms melting. In addition, the critical melt flow velocity corresponding to the melting of dendritic arm becomes smaller as the temperature gradient decreases and the growth rate increases, according to Eq. (16).

### 4.1.4 Survival of free crystal nuclei

As mentioned earlier, the following parameters were used to describe the solidification process: undercooling of $\Delta T$, cooling rate of $R$, temperature gradient of $G$, and growth rate of $V$. The mold shape parameter, $r$, is defined as the distance between the initial and final positions of the solidification front. In the case of a cylindrical ingot, this parameter is closely approximated by the ingot's radius. Assuming that these parameters do not change with time, the total solidification time $t_{total}$ can be represented by Eq. (17):

$$t_{total} = \frac{r}{v} \tag{17}$$

Campanella[25] believes that dendrite fragments enter the liquid phase from the mushy zone and eventually become nuclei, leading to grain refinement. The flow velocity component in the temperature gradient direction must be greater than the dendrite growth rate; that is, fluid flow can bring dendrite fragments to the front of the solid-liquid interface, forming additional dendrites. This flow velocity is the sum of natural convection and forced convection caused by PMF. Meanwhile, the crystal nuclei generated by the PMF can survive in melts with temperatures below the liquidus temperature, $T_m$, but cannot survive at high temperatures. Assuming that the velocity parallel to the temperature gradient direction of a certain dendritic fragment is $u$, and at $t$=0, there is a dendritic fragment at the front of the mushy zone, the sufficient condition for the fragment to survive is that the conditions and survival temperature conditions given by Campanella should be met throughout the entire solidification stage, i.e. $t=L/V$, corresponding to Eqs. (18) and (19), respectively:

$$u > V \tag{18}$$

$$\mu \cdot (L/V) \cdot G + T_m - \Delta T - R(L/V) < T_m \tag{19}$$

where $L$ represents the characteristic size of the casting from the initial solidification area to the final solidification area, $\Delta T$ is the undercooling at the front of the dendrite.

The conditions for the survival of dendritic fragments are summarized as Eq. (20):

$$\frac{R}{G}<u<[\frac{\Delta T}{GL}+1]\frac{R}{G} \quad (20)$$

According to Eq. (20), if the dendritic fragments can survive, their motion speeds need to meet a specific range. In fact, due to the continuous growth of dendritic fragments in undercooled melts and the time required for dendritic fragment remelting, the upper limit of the melt flow velocity that satisfies the survival of dendritic fragments should be higher than the value given in Eq. (20). When the cooling rate $R$ is constant, this range increases with a decrease in temperature gradient $G$. When the temperature gradient $G$ is constant, this range increases with an increase in cooling rate $R$. In addition, an increase in undercooling at the front of the dendrite also leads to a rise of this range. The range of melt flow velocities corresponding to the survival of dendrite fragments becomes wider as the cooling rate $R$ increases, the temperature gradient $G$ decreases, and the undercooling at the dendrite front increases. Simultaneously, the melt flow velocity required for the survival of dendrite fragments is also higher.

To investigate the survival of nuclei, a near-liquid phase insulation quenching method was adopted. A $\Phi$8 mm×50 mm rod was heated to 1,600 °C, and then slowly cooled to near liquidus for 20 min under the action of PMF. After slowly cooling, the sample was quenched in water, and the solidified structure after quenching is shown in Fig. 10. There is a temperature gradient along the vertical direction of the sample, in which the temperature increases sequentially from the bottom to the top. By comparing the solidification structure with and without the application of PMF, the sample can be divided into three regions, as shown in Fig. 10. Region I is a mushy zone, in which the dendritic morphologies are observed in the quenched solid phases. Without applying PMF, the primary solid phases develop into dendritic morphology, as shown in Fig. 10(f). After applying PMF, the morphology of dendrites in the primary solid phase deteriorates. There is a tendency for fracture at the root of the secondary arm. The primary solid phases evolve into fine dendrites after quenching, as shown in Fig. 10(g). Both Regions II and III are pure liquid regions without primary phases in the melt. In Region II, the microstructure of the quenched melt exhibits developed dendritic crystals, as shown in Fig. 10(d), with a number density of crystal nuclei of about 0.2 $mm^{-2}$ without PMF. After applying PMF, the microstructure of the quenched melt is significantly refined and some dendrites with significant differences from the quenched microstructure appear, as shown by the circles in Fig. 10(e). These dendrites exhibit obvious upstream growth characteristics. The number density of crystal nuclei in this area increases to approximately 6.0 $mm^{-2}$. In Region III, regardless of whether a PMF is applied or not, the microstructure of the quenched melt exhibits well-developed dendrites, as shown in Figs. 10(a) and (b).

Due to the rapid quenching process and the large distance between the sample and the PMF excitation coil, the PMF intensity is very weak. Therefore, the crystal nuclei that proliferate in Region II are more likely to be formed during the insulation stage rather than the quenching stage. In addition, due

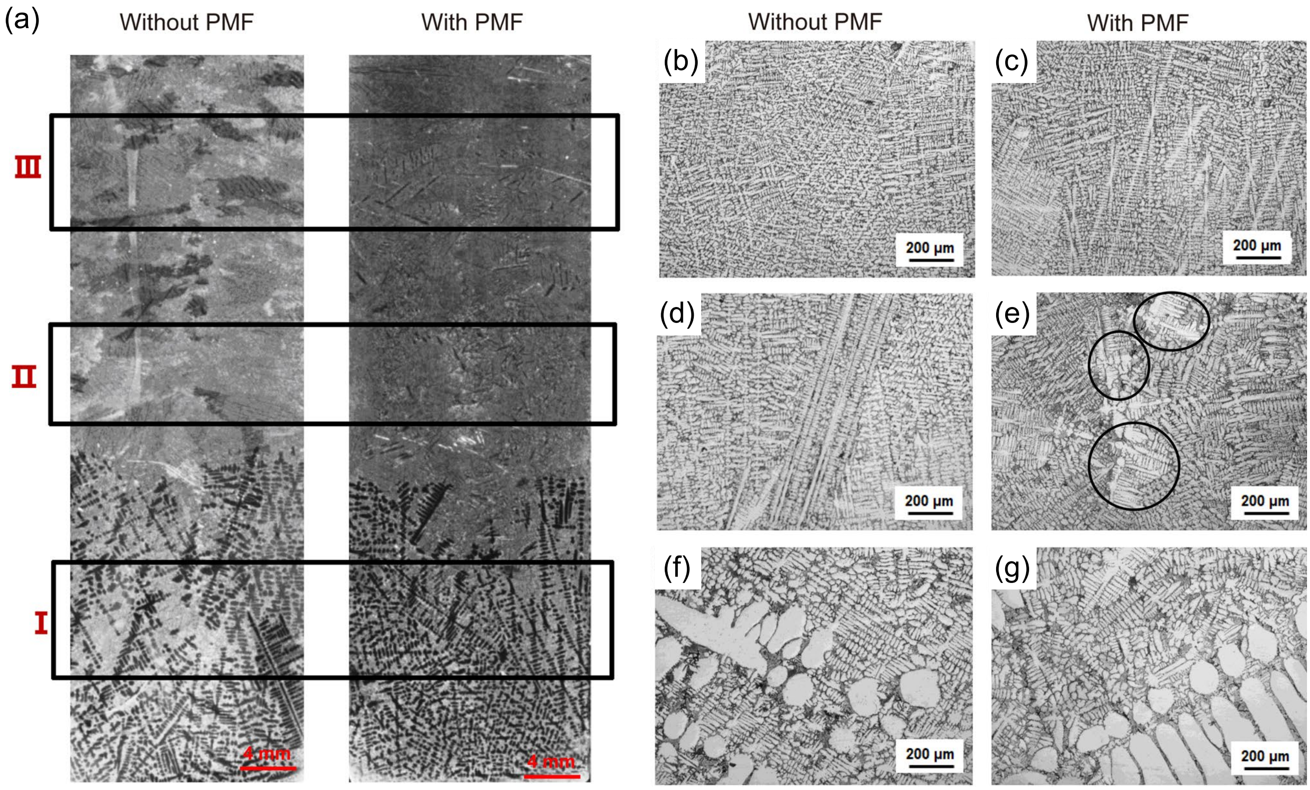


**Fig. 10: Solidification structures of quenched specimen: (a) macrostructures of samples without and with a PMF of 5 Hz, 200 V; (b, c) microstructures of Region III; (d, e) microstructures of Region II; (f, g) microstructures of Region I**

to the insulation process of the sample, it can be considered that the undercooling of the solid phase in Region I is very small at the forefront of the vertical direction, and the temperature is very close to the liquidus. Therefore, there is a certain temperature gradient in the sample from bottom to top. Based on the quenching experiment results, the following conclusions can be drawn: under the action of PMF, crystal nuclei dissociate to the front of the solid-liquid interface and survive in melts with temperatures below or slightly above the liquidus. When the temperature is too high, they cannot survive. Therefore, in Eq. (19), the term to the right of the equation should be $T_m+\Delta T_{survive}$; and $\Delta T$ should be $\Delta T+\Delta T_{survive}$ in Eq. (20).

The aforementioned analysis on crystal nucleus proliferation and dendrite fragmentation suggests that the melt flow is the key factor for grain refinement. The characteristic melt flow velocity under the action of PMF is $u$, and the probability density function of flow velocity in the entire melt is $f(u)$. According to the definition of the probability density function, the properties of $f(u)$ are described by following equation system (21):

$$\begin{cases} f(u) \geq 0 \\ \int_0^{+\infty} f(u) = 1 \\ P(a < u \leq b) = \int_a^b f(u) \end{cases} \tag{21}$$

Within the time of $\Delta t$, the growth length of dendrites is $V\Delta t$. The number of dendritic arms generated in the entire casting, $N_{total}$, can be approximately represented by Eq. (22):

$$N_{total} = k\frac{V\Delta t}{\lambda} \tag{22}$$

where $k$ is the undetermined coefficient correlated to the volume of melt, $\lambda$ is dendritic arm spacing.

According to the criterion of dendrite fragmentation, the number of dendritic fragments $N_{fracture}$ within the time of $\Delta t$ is represented by Eq. (23):

$$N_{fracture} = N_{total} \cdot \int_{u_{crit}}^{+\infty} f(u)$$
$$u_{crit} = k_{fracture} G^{n_5} V^{n_6} \approx \text{const} \tag{23}$$

Among these dendritic arms, the number of surviving dendritic arms $N_{survive}$ is expressed as Eq. (24):

$$N_{survive} = N_{fracture} \cdot \int_{u_{min}}^{u_{max}} f(u)$$
$$u_{min}=R/G,\ u_{max}=[(\Delta T+\Delta T_{survive})/(GL)+1]R/G \tag{24}$$

Therefore, based on the theory of dendritic arm fragmentation and free survival, a schematic diagram of the influence of cooling conditions and pulse parameters on the refinement effect is shown in Fig. 11. Under the conditions

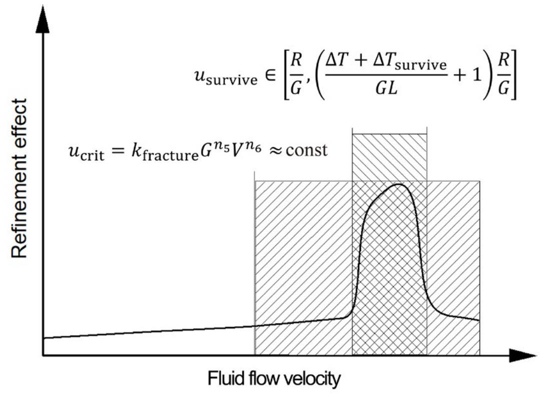


**Fig. 11: Effect of cooling conditions and forced fluid flow on grain refinement under PMF based on assumption of dendrites fragment and survival**

of cooling rate $R$ and temperature gradient $G$, the number of surviving dendritic fragments throughout the entire solidification stage is expressed as Eq. (25):

$$N_{survive} = k\frac{RL}{\lambda G^2} \cdot \int_{u_{min}}^{u_{max}} f(u) \cdot \int_{u_{crit}}^{+\infty} f(u) \tag{25}$$

where $k\frac{RL}{\lambda G^2}$ represents the number of possible dendritic arms that may form dendritic fragments, $\int_{u_{min}}^{u_{max}} f(u)$ represents the survival probability of dendritic arms, and $\int_{u_{crit}}^{+\infty} f(u)$ represents the breakage probability of dendritic arms.

In summary, the number of surviving dendrite fragments increases with an increase in cooling rate and undercooling at the front of dendrites, and a decrease in temperature gradient and dendrite spacing. The breakage probability of dendritic arms is related to the melt flow velocity. The survival of dendritic arms requires a moderate melt flow velocity, which is related to the cooling conditions of the melt. Overall, the number of surviving dendritic fragments shows a trend of first increase and then decrease with an increase in melt flow velocity. Therefore, applying PMF increases the number of surviving dendritic fragments, resulting in a grain refinement effect. However, as shown in Fig. 11, when the cooling conditions of the melt result in a narrow overlap between the speed ranges for dendritic arm breakage and dendritic arm survival, it becomes challenging to achieve significant grain refinement through the application of a PMF. This is particularly true under conditions of slow cooling rates and large temperature gradients.

## 4.2 Suitable thermal conditions for grain refinement

From the quenching experiment in Fig. 10, it can be seen that more heterogeneous nuclei are generated by PMF. Grain refinement can occur if there is a sufficiently large melt zone with a low level of superheat in front of the dendrites, allowing heterogeneous nuclei to survive and develop into grains. To analyze the thermal conditions under the pouring temperature of 1,550 °C, two sets of thermal couples were adopted to measure the cooling curves of the melt and the mold on the transverse section. One set of thermocouples was positioned along the central axis of the melt. The other set was located on the exterior surface of the investment mold, approximately 10 mm away from the surface of the cylindrical ingot. The cooling curves of the melt and the mold are shown in Fig. 12. The cooling rate between $T_{liquid}$ and $T_{solid}$ is much slower (about 0.1 °C·s$^{-1}$) than that in Ma's research[15] (about 10 °C·s$^{-1}$ from $T_{liquid}$ to 1,300 °C and 1 °C·s$^{-1}$ from 1,300 °C to $T_{solid}$).

The thermal gradient from the center to the side of the ingot was analyzed as follows. By neglecting the convection and interface thermal resistance, the average heat flux in the melt ($H_{fluxmelt}$, W·m$^{-2}$) and in the mold ($H_{fluxmold}$, W·m$^{-2}$) at a time are calculated as Eqs. (26) and (27):

$$H_{\mathrm{fluxmelt}} = \lambda_{\mathrm{melt}} (T_{\mathrm{melt}} - T_{\mathrm{interface}}) / L_{\mathrm{melt}} \qquad (26)$$

$$H_{\mathrm{fluxmold}} = \lambda_{\mathrm{mold}} (T_{\mathrm{interface}} - T_{\mathrm{mold}}) / L_{\mathrm{mold}} \qquad (27)$$

where $\lambda_{melt}$ and $\lambda_{mold}$ are the heat conductivity of the melt and the mold (31.0 W·m$^{-1}$·°C$^{-1}$ and 1.9 W·m$^{-1}$·°C$^{-1}$, respectively[26]), $T_{melt}$ and $T_{mold}$ are the temperatures at two measuring points obtained from the cooling curves in Fig. 12, $L_{melt}$ and $L_{mold}$ denote the length between the interface to the two measuring points (0.025 and 0.01 m, respectively).

As the cooling rate is slow, it is reasonable to consider that the heat flux in the melt and the mold is the same. The temperature gradient in the melt can be easily deduced and plotted in a dotted line in Fig. 12. The thermal gradient of the melt under the pouring temperature of 1,550 °C is about 1–2 °C·mm$^{-1}$ during solidification based on the above derivation. Moreover, the actual thermal gradient should be smaller, considering that natural convection and forced convection driven by a PMF homogenate the melt temperature[16]. Consequently, the thermal gradient in the melt is adequately small so that when the dendrites in the coldest region of the melt begin to grow, the heterogeneous nuclei generated by the PMF can survive and grow within a large area of melt in front of the dendrites. More heterogeneous nuclei can be further generated in the refined structure, resulting in significant grain multiplication under a PMF. Consequently, the solidification structure is finally well-refined.

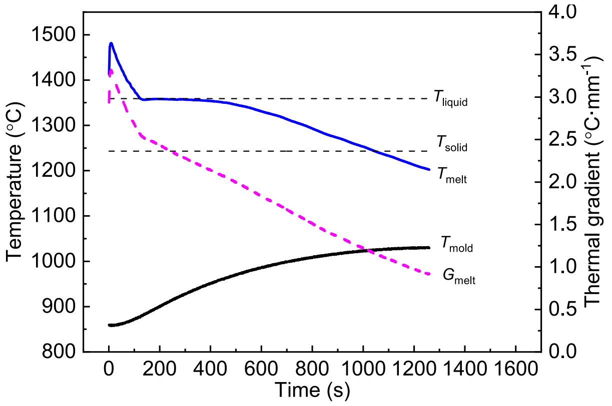


**Fig. 12: Cooling curves and thermal gradient under pouring temperature of 1,550 °C**

## 4.3 Effect of PMF on dendritic morphology of K4169 superalloy

The mechanism for the influence of PMF on the dendritic morphology of as-cast solidification structure is as follows: firstly, the number of crystal nuclei increases under the action of PMF, resulting in each dendrite having insufficient time to grow fully before approaching neighboring dendrites. As shown in Fig. 1(c), the entire solidification structure of the ingot is composed of equiaxed crystals. The undercooled melt around the dendrites absorbs the solidification latent heat released by equiaxed crystals. Therefore, the increase in number of grains leads to mutual thermal diffusion effects during dendrite growth. This interaction hinders the release of solidification latent heat, reduces the growth rate, and increases the secondary arm spacing [Eq. (10)]. Furthermore, according to the LMK interface stability theory[27], the relationship between growth rate and dendrite tip radius satisfies Eq. (28):

$$V^2 r_{\mathrm{d}} = \frac{8\pi^2 D_{\mathrm{L}} \Gamma}{m_{\mathrm{L}} C_0 (k_0 - 1)} \qquad (28)$$

where $V$ is the growth rate of dendrites, $r_d$ is the tip radius of the dendrite, $D_L$ is the diffusion coefficient of solute in the liquid phase, $\Gamma$ is the Gibbs-Thompson coefficient, $m_L$ is the slope of the liquidus, $C_0$ is the initial composition of alloy, and $k_0$ is the solute equilibrium distribution coefficient.

For a given alloy, the right-hand side of Eq. (28) can be considered to be constant. Under the action of PMF, the radius of the dendrite tip increases due to the decrease in growth rate, resulting in passivation of the dendrite tip.

Secondly, the PMF generates forced convection and oscillation effects in the melt during the solidification process, causing the dendritic arms to break, promoting the maturation process of the dendrites, and leading to an increase in the spacing between the secondary arms.

Thirdly, the Joule heating effect generated by PMF concentrates at the roots and tips of dendrites with sudden curvature changes, causing remelting of dendrite tips and melting of dendrite roots. The above three reasons may lead to the degradation of dendritic morphology and an increase in secondary dendritic arm spacing.

Similar changes in dendritic morphology were also observed in the study of refining K4169 superalloy using a refiner, without the influence of forced convection, oscillation, or thermal effects during the solidification process[28]. In addition, the oscillation, convection, and thermal effects of the PMF gradually increase as the pulse voltage and frequency increase. However, according to Figs. 3 and 6, the degree of dendrite morphology degradation does not conform to the aforementioned trend at a pulse voltage of 70 V and frequency of 5 Hz, or at 200 V and 10 Hz. Referring to Figs. 1 and 4, the degradation of dendrite morphology exhibits a similar pattern to the refinement of solidification structure under the action of different pulse parameters. Therefore, it may be the main reason for the changes in dendrite morphologies under the action of PMF, that is, the PMF causes grain refinement and subsequently leads to dendrite passivation.

### 4.4 Effect of pulse frequency and pulse voltage on grain refinement of K4169 superalloy

The results presented in Figs. 1 and 2 indicate that the grain sizes of the K4169 alloy decrease within the pulse frequency range of 0 to 5 Hz at a fixed pulse voltage of 200 V. However, they exhibit an increase at a pulse frequency of 10 Hz. A high pulse frequency is not considered an advantageous technological parameter for achieving grain refinement through PMF[29]. The thermal effect generated by the PMF is primarily concentrated on the mold wall, which hinders the survival of free nuclei that have detached from the wall. Consequently, nucleation inhibition due to the thermal effect becomes more significant when the pulse frequency exceeds the optimal frequency of 5 Hz. Therefore, PMF with a pulse frequency of 10 Hz does not enhance grain refinement.

In addition, a practical grain refinement is observed when the pulse voltage is over 70 V at a fixed pulse frequency of 5 Hz, as shown in Fig. 4. At the same time, the grain sizes decrease with increasing the pulse voltage (Fig. 5). As the voltage increases, both magnetic vibration and melt convection are notably enhanced, which facilitates dendrite fragmentation and reduces the temperature gradient in front of the solid-liquid interface. Consequently, as the pulse voltage increases, the grains undergo refinement.

## 5 Conclusions

Solidification experiments combined with theoretical analysis were used to analyze the refining mechanism of the grain microstructure of K4169 superalloy by PMF, especially the reason why a PMF can produce a significant refining effect at a high pouring temperature of 1,550 °C. The reasons and necessary conditions for grain refinement caused by PMF were discussed in detail, as well as the influence of pulse parameter changes on the grain refinement effect. The main conclusions are summarized as follows:

(1) The refinement effect of the pulsed magnetic field (PMF) exhibits an increasing trend with pulse voltages ranging from 70 to 200 V at a pulse frequency of 5 Hz. At a high pouring temperature of 1,550 °C, the refinement effect firstly increases and then decreases as the pulse frequency increases at a pulse voltage of 200 V. The optimal refinement effect is achieved with a frequency of 5 Hz and a pulse voltage of 200 V, reducing the average grain size of the ingot from 3.9 mm (without PMF) to 1.7 mm.

(2) The refinement mechanism of PMF was investigated by liquid quenching experiments at different stages, combined with theoretical analysis. The main stage for refining grains with PMF is the solidification plateau stage of liquid-solid transformation. The PMF provides free energy for the nucleation process.

(3) A crystal nucleus proliferation model was established based on the assumption of dendrite fragmentation and free survival of dendrite fragments caused by melt flow:

$$\begin{cases} u > k_{\text{fracture}} G^{n_5} V^{n_6} \\ \dfrac{R}{G} < u < \left[ \dfrac{\Delta T + \Delta T_{\text{survive}}}{GL} + 1 \right] \dfrac{R}{G} \end{cases}$$

(4) Under the action of PMF, the morphologies of dendrites deteriorate, resulting in incomplete dendrites, blunt tips, and increased secondary arm spacing. The pulse frequencies and pulse voltages have little effect on the degradation of dendrite morphologies.

(5) By applying the PMF, the solidification structure can be refined even at high superheat, ensuring good filling ability and finer grain size simultaneously, which has prospects in practical application for thin-walled complex parts.

## Acknowledgments

The authors acknowledge the financial support by the National Key Research and Development Program (No. 2018YFA0702900), the National Science and Technology Major Project (No. J2019-VII-0002-0142), and the National Natural Science Foundation of China (No. 51831007).

## Conflict of interest

The authors declare that they have no conflict of interest.

## References

[1] Wang Y, He J, Hu P, et al. Exceptional cryogenic tensile properties of K4169 superalloy by micro-grain casting process. Materials & Design, 2023, 236: 112450.

[2] Liu L, Huang T, Xiong Y, et al. Grain refinement of superalloy K4169 by addition of refiners: Cast structure and refinement mechanisms. Materials Science and Engineering: A, 2005, 394(1–2): 1–8.

[3] Ma Y, Sun J, Xie X, et al. An investigation on fine-grain formation and structural character in cast IN718 superalloy. Journal of Materials Processing Technology, 2003, 137(1–3): 35–39.

[4] Asai S. Recent development and prospect of electromagnetic processing of materials. Science and Technology of Advanced Materials, 2000, 1(4): 191–200.

[5] Li Q, Li H, Zhai Q. Structure evolution and solidification behavior of austenitic stainless steel in pulsed magnetic field. Journal of Iron and Steel Research International, 2006, 13(5): 69–72.

[6] Bao L, Zhao D, Zhao Y, et al. Effect of harmonic magnetic field and pulse magnetic field on microstructure of high purity Cu during electromagnetic direct chill casting. China Foundry, 2021, 18(2): 141–146.

[7] Li Q, Li L, Chang G, et al. Effects of pulsed current and pulsed magnetic field complex pretreatment on martensite transformation of Cr5 steel during continuous cooling. Journal of Iron and Steel Research International, 2015, 22(12): 1131–1137.

[8] Li Q, Song C, Li H, et al. Effect of pulsed magnetic field on microstructure of 1Cr18Ni9Ti austenitic stainless steel. Materials Science and Engineering: A, 2007, 466(1–2): 101–105.

[9] Gao Y L, Li Q S, Gong Y Y, et al. Comparative study on structural transformation of low-melting pure Al and high-melting stainless steel under external pulsed magnetic field. Materials Letters, 2007, 61(18): 4011–4014.
[10] Bin W, Yang Y, Zhou J, et al. Microstructure refinement of AZ91D alloy solidified with pulsed magnetic field. Transactions of Nonferrous Metals Society of China, 2008, 18(3): 536–540.
[11] Li Y J, Tao W Z, Yang Y S. Grain refinement of Al-Cu alloy in low voltage pulsed magnetic field. Journal of Materials Processing Technology, 2012, 212(4): 903–909.
[12] Li Y J, Teng Y F, Yang Y S. Refinement mechanism of low voltage pulsed magnetic field on solidification structure of silicon steel. Metals and Materials International, 2014, 20: 527–530.
[13] Ma X, Li Y, Yang Y. Grain refinement effect of a pulsed magnetic field on as-cast superalloy K417. Journal of Materials Research, 2009, 24(8): 2670–2676.
[14] Zhang K, Li Y, Yang Y. Simulation of the influence of pulsed magnetic field on the superalloy melt with the solid-liquid interface in directional solidification. Acta Metallurgica Sinica (English Letters), 2020, 33: 1442–1454.
[15] Ma X, Li Y, Yang Y. Grain refinement effect of a pulsed magnetic field on as-cast superalloy K417. Journal of Materials Research, 2009, 24(8): 2670–2676.
[16] Li Y J, Yang Y. Grain refinement of as-cast superalloy IN718 under action of low voltage pulsed magnetic field. Transactions of Nonferrous Metals Society of China, 2011, 21(6): 1277–1282.
[17] Liotti E, Lui A, Vincent R, et al. A synchrotron X-ray radiography study of dendrite fragmentation induced by a pulsed electromagnetic field in an Al-15Cu alloy. Acta Materialia, 2014, 70: 228–239.
[18] Ma X, Li Y, Yang Y. The origin of nuclei and the refinement mechanism for solidified superalloy IN718 under pulsed magnetic field. Journal of Materials Research, 2009, 24(12): 3689–3692.
[19] Jie Z Q, Zhang J, Huang T W. et al. Effects of grain refinement on cast structure and tensile properties of superalloy K4169 at high pouring temperature. China Foundry, 2016, 3(2): 101–106.
[20] Asai S. Electromagnetic processing of materials. Berlin: Springer, 2012: 1–6.
[21] Nastac L, Stefanescu D M. Macrotransport-solidification kinetics modeling of equiaxed dendritic growth: Part II. Computation problems and validation on INCONEL 718 superalloy castings. Metallurgical and Materials Transactions: A, 1996, 27(12): 4075–4083.
[22] Kurz W. Fundamentals of solidification, 4th revised edition. Beijing: Higher Education Press, 2010: 74.
[23] Flemings M C. Behavior of metal alloys in the semisolid state. Metallurgical Transactions: B, 1991, 22: 269–293.
[24] Dahle A K, Arnberg L. Development of strength in solidifying aluminium alloys. Acta Materialia, 1997(45): 547–559.
[25] Campanella T, Charbon C, Rappaz M. Grain refinement induced by electromagnetic stirring: A dendrite fragmentation criterion. Metallurgical & Materials Transactions: A, 2004, 35: 3201–3210.
[26] Holman J P. Heat transfer. New York: McGraw-Hill, 2010: 653.
[27] Langer J S, Müller-Krumbhaar H. Theory of dendritic growth– I. Elements of a stability analysis. Acta Metallurgica, 1978, 78: 281–287.
[28] Xiong Y H, Li P J, Yang A M, et al. Effects of foundry variables and refiners on cast structures of superalloy K4169: II. Grain structures and grain spheroidization mechanisms. Acta Metallrugica Sinica, 2002, 38(5): 534–538. (In Chinese)
[29] Bin W, Yang Y, Sun M. Microstructure refinement of AZ31 alloy solidified with pulsed magnetic field. Transactions of Nonferrous Metals Society of China, 2010, 20(9): 1685–1690.